Eleventh U.S. National Conference on Earthquake Engineering
Integrating Science, Engineering & Policy
June 25-29, 2018
Los Angeles, California

USE OF AIRBORNE SAR IMAGERY TO EXTRACT EARTHQUAKE DAMAGE IN URBAN AREAS

F. Yamazaki[1], W. Liu[2] and S. Kojima[3]

ABSTRACT

Extensive impacts due to strong shaking and landslides were caused by the 2016 Kumamoto, Japan, earthquake sequence, such as collapse of buildings and bridges. Soon after the occurrence of the earthquake, the National Institute of Information and Communications Technology (NICT), Japan, observed affected areas by Pi-SAR2, an airborne X-band SAR sensor. Using the full-polarimetric (HH, HV, VV and VH) Pi-SAR2 data and a 4-component covariance matrix decomposition method, the backscattering characteristics of the affected urban area were investigated. The result of the analysis was compared with a damage distribution map obtained by field surveys and airborne LiDAR data. Based on the comparison, radar shadows and layover areas of the Pi-SAR2 data for collapsed wooden houses were seen to be unclear and with irregular shapes, compared with solid undamaged buildings. But more information may be necessary until the extraction of collapsed buildings only from a single SAR image is performed.

[1]Professor, Dept. of Urban Environment Systems, Chiba University, Chiba 263-8522, Japan
(email: fumio.yamazaki@faculty.chiba-u.jp)
[2]Assistant Professor, Dept. of Urban Environment Systems, Chiba University, Chiba 263-8522, Japan
[3]Research Manager, National Institute of Information and Communications Technology, Tokyo 184-8795, Japan

Yamazaki F, Liu W, Kojima S. *Proceedings of the 11th National Conference on Earthquake Engineering*, Earthquake Engineering Research Institute, Los Angeles, CA. 2018.

Eleventh U.S. National Conference on Earthquake Engineering
Integrating Science, Engineering & Policy
June 25-29, 2018
Los Angeles, California

Use of airborne SAR imagery to extract earthquake damage in urban areas

F. Yamazaki[1], W. Liu[2] and S. Kojima[3]

ABSTRACT

Extensive impacts due to strong shaking and landslides were caused by the 2016 Kumamoto, Japan, earthquake sequence, such as collapse of buildings and bridges. Soon after the occurrence of the earthquake, the National Institute of Information and Communications Technology (NICT), Japan, observed affected areas by Pi-SAR2, an airborne X-band SAR sensor. Using the full-polarimetric (HH, HV, VV and VH) Pi-SAR2 data and a 4-component covariance matrix decomposition method, the backscattering characteristics of the affected urban area were investigated. The result of the analysis was compared with a damage distribution map obtained by field surveys and airborne LiDAR data. Based on the comparison, radar shadows and layover areas of the Pi-SAR2 data for collapsed wooden houses were seen to be unclear and with irregular shapes, compared with solid undamaged buildings. But more information may be necessary until the extraction of collapsed buildings only from a single SAR image is performed.

Introduction

Information gathering after a large-scale natural disaster strikes is important in emergency response and recovery activities. But the access to the affected areas is often hindered by the disruption of road networks and telecommunication systems. Thus remote sensing technologies have been employed to assess the extent and degree of various damages [1-5]. Various high-resolution optical and Synthetic Aperture Radar (SAR) satellites have been in operation in the recent years and they were employed to observe affected areas after major natural disasters such as the 2011 Tohoku, Japan, earthquake and tsunami [6], the 2011 central Thailand flood [7], and the 2015 Gorkha, Nepal, earthquake [8]. The acquired satellite data provided the information on inaccessible affected areas.

[1]Professor, Dept. of Urban Environment Systems, Chiba University, Chiba 263-8522, Japan (email: fumio.yamazaki@faculty.chiba-u.jp)
[2]Assistant Professor, Dept. of Urban Environment Systems, Chiba University, Chiba 263-8522, Japan
[3]Research Manager, National Institute of Information and Communications Technology, Tokyo 184-8795, Japan

Yamazaki F, Liu W, Kojima S. *Proceedings of the 11th National Conference on Earthquake Engineering*, Earthquake Engineering Research Institute, Los Angeles, CA. 2018.

SAR sensors can be used all day and under all weather conditions, and hence they are suitable for emergency data acquisition. Several frequency bands have been commonly used for satellite SAR systems, such as L-band (1 - 2 GHz: JERS-1, ALOS_PALSAR, ALOS-2_PALSAR-2), C-band (4 - 8 GHz: ERS-1/2, ENVISAT, Radarsat-1/2, RISAT-1, Sentinel-1), and X-band (8 - 12 GHz: TerraSAR-X, COSMO-SkyMed). Among these frequency bands, the L-band is suitable to observe coherent changes such as ground deformation while the X-band is suitable to observe manmade objects and small-scale changes.

In the recent years, airborne SAR systems have also been developed and used as an experimental phase. The Japan Aerospace Exploration Agency (JAXA) operated airborne L-band SAR systems, Pi-SAR-L (Polarimetric and Interferometric Airborne Synthetic Aperture Radar) from 1996 to 2011 and Pi-SAR-L2 from 2012 to 2016 [9, 10] and acquired scenes were used for land use/cover classification analyses [11]. The National Institute of Information and Communications Technology, Japan (NICT) has been operating airborne X-band SAR systems, Pi-SAR and its successor, Pi-SAR2 [12, 13], on the common airplane with JAXA. Pi-SAR2 has a very high-resolution mode (0.3 m) with full polarization (HH, HV, VV and VH).

In this paper, Pi-SAR2 data acquired just after the main-shock of the 2016 Kumamoto, Japan, earthquake is employed to investigate the capability of the X-band airborne SAR data in damage extraction of urban areas. The result of analysis is compared with a damage distribution map obtained by field surveys and airborne LiDAR data.

The 2016 Kumamoto Earthquake Sequence

An Mw6.2 earthquake hit the Kumamoto prefecture in Kyushu Island, Japan, on April 14, 2016 at 21:26 (JST). A considerable amount of structural damages and human casualties had been reported due to this event, including 9 deaths. The epicenter was located in the Hinagu fault with a shallow depth. On April 16, 2016 at 01:25 (JST), about 28 hours after the first event, another earthquake of Mw7.0 occurred in the Futagawa fault, closely located with the Hinagu fault. Thus, the first event was called as the "foreshock" and the second one as the "main-shock". The epicenters of the both events were located in Mashiki Town (about 33-thousand population), to the east of Kumamoto City (about 735-thousand population).

Figure 1 shows the location of these causative faults and Japanese national GNSS Earth Observation Network System (GEONET) stations in the source area [14]. The displacement of 75 cm to the east-northeast (ENE) was observed at the Kumamoto station while that of 97 cm to the southwest (SE) was recorded at the Choyo station during the main-shock. These observations are consistent with the right-lateral strike-slip mechanism of the Futagawa fault. The peak ground acceleration (PGA) and the peak ground velocity (PGV) recorded at the KiK-net Mashiki station (KMMH16) were 925 cm/s^2 and 92 cm/s in the foreshock while those were 1,313 cm/s^2 and 132 cm/s in the main-shock [15].

Extensive impacts due to strong shaking and landslides were associated by the Kumamoto earthquake sequence, such as collapse of buildings and bridges, and suspension of road and railway networks. A total of fifty (50) direct deaths were accounted by the earthquake sequence, mostly due to the collapse of wooden houses in Mashiki Town and landslides in Minami-Aso Village. The present authors have conducted field investigations for several times [16, 17] and analyzed satellite SAR data [18, 19] and LiDAR data [20, 21].

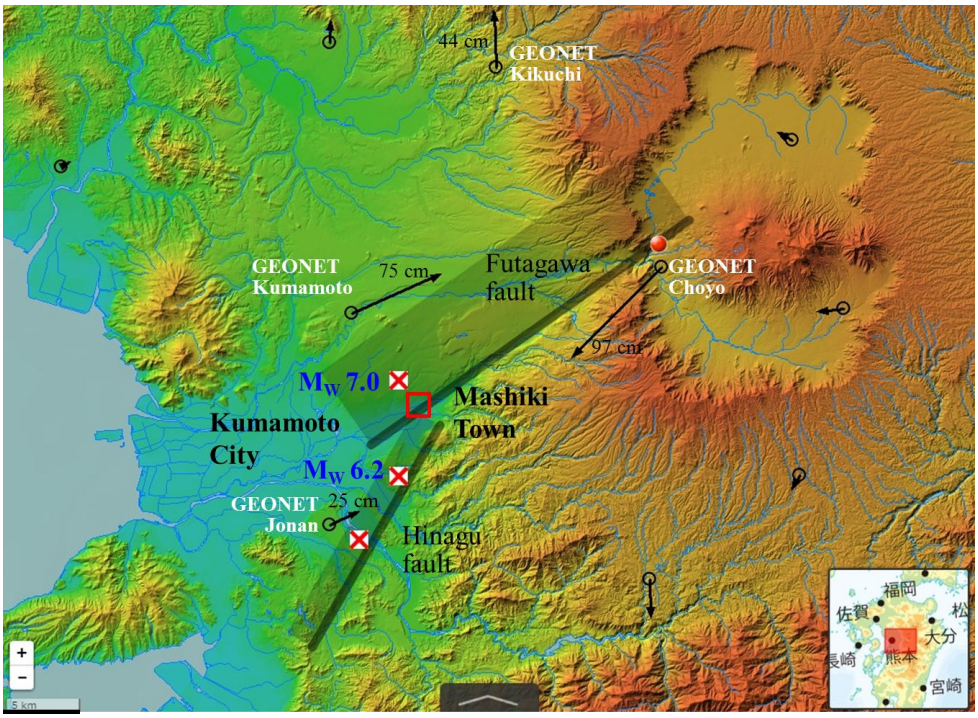

Figure 1. Location of causative faults and GEONET stations in the 2016 Kumamoto earthquake. Red square shows the study area of Pi-SAR2 data.

Pi-SAR2 Data after the Kumamoto Earthquake

The second generation airborne polarimetric and interferometric synthetic aperture radar system (Pi-SAR2) was designed and developed by National Institute of Information and Communications Technology (NICT), Tokyo, Japan from 2006 to 2009, as a successor to the Pi-SAR. Table 1 summarizes the specifications of Pi-SAR and Pi-SAR2 radar sensors.

Table 1.Comparison of specifications of Pi-SAR and Pi-SAR2 [12]

Parameter	**Pi-SAR**	**Pi-SAR2**
Center frequency	9.55 GHz	9.65/9.55 GHz
Bandwidth	100 MHz	500/300/150 MHz (in modes)
Slant range resolution	1.5 m	0.3/0.5/1.0 m
Azimuth resolution	1.5 m (4 looks)	0.3 m (1 look) / 0.6 m (2 looks)
Swath width	> 10 km	> 5 -10 km
NESZ (Noise Equivalent Sigma Zero)	< -33 dB	< -23/ -27/ -30 dB
Source data rate	32 MB/s x 2 channels	200 MB/s x 4 channels
Data recorder	D1 tape recorder x 2 channels	3.5 inch HD array x 4 channels
Radome location	Fore part of body	base of wings
Distance between main and sub antenna	2.3 m	2.6 m
Antenna azimuth movement	-	sliding spotlight (optional mode)

The PiSAR-2 onboard a Culfstream-II jet plane observed the affected area of the Kumamoto earthquake in the morning (8:15-10:15 am) of April 17, 2017, one day after the main-shock, from the altitude of 9,000 m. The central part of Mashiki Town (shown in the red square in Fig. 1) including the town-hall was chosen as the study area of the post-event Pi-SAR2 data. The heading angle of the flight path was 83.04 degrees (east to west) clockwise from the north with the left look.

First the original full-polarimetric Pi-SAR2 data were decomposed into the 4-component scattering power, which means the double-bounce scattering (P_d), volume scattering (P_v), surface scattering (P_s), Helix scattering (P_c). The decomposition was carried out using the PolSARpro_v5.1 software [22] developed by the European Space Agency (ESA). The general 4-component scattering power decomposition using the Unitary transformation of the coherency matrix (G4U) was adopted as the decomposition method [23].

Figure 2 compares the color composite of the G4U Pi-SAR2 data and an aerial photograph (taken by Asia Air Survey Co., Ltd [24] together with LiDAR data on April 23, 2017) of the central part of Mashiki Town. To produce a clear image, the scattering power was converted to its logarithm in the figure, where built-up urban areas can be clearly distinguished from the surrounding agricultural lands. Note that although airborne SAR images have very high-spatial resolution, it is difficult to acquire multi-temporal images with the same observation conditions. Thus the coherence or correlation analysis [18] for two-temporal images cannot be applied. In this situation, only a single post-earthquake SAR image must be used in the extraction of building damage areas.

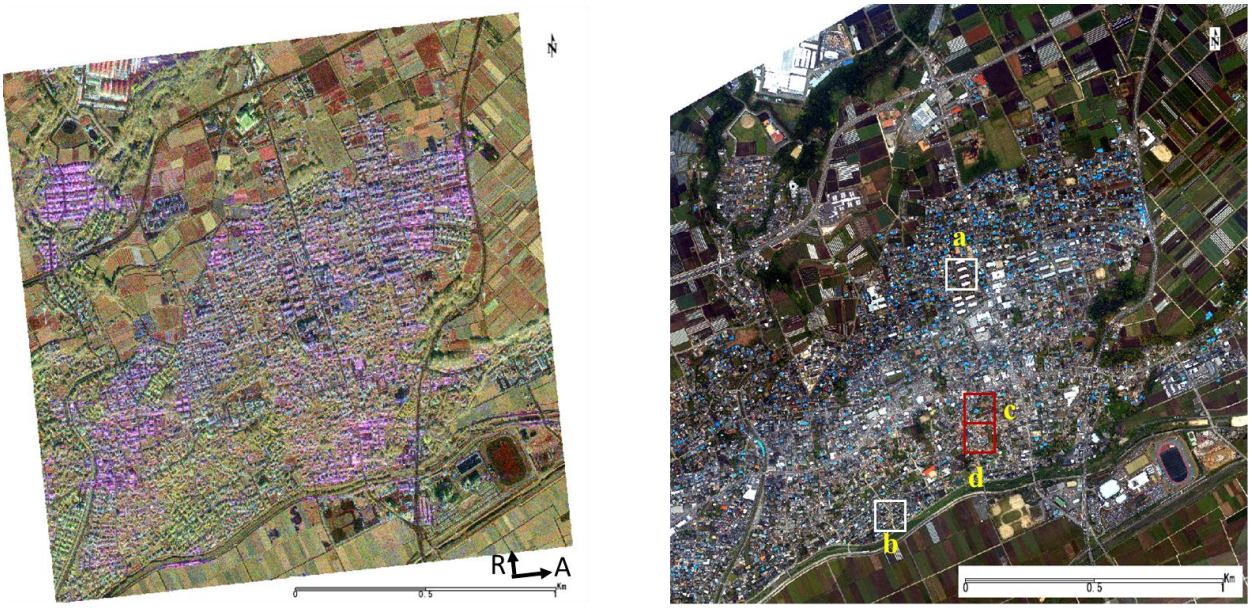

(a) Pi-SAR2 color composite on 2016/04/17 (b) Asia Air Survey's aerial photo on 2016/04/23

Figure 2. Color composite of full polarimetric Pi-SAR2 data (a) and the aerial photo (b) of the central part of Mashiki Town.

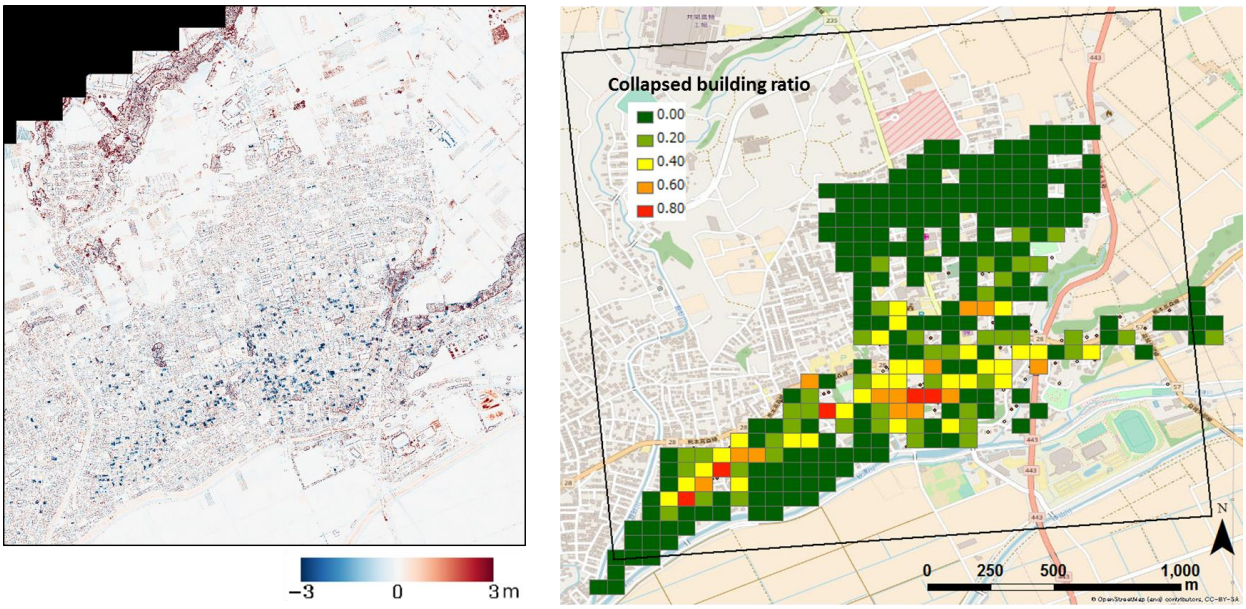

(a) Height difference of Lidar DSMs

(b) Collapsed building ratio in 57 m x 57 m grid by AIJ's survey

Figure 3. Height difference [20] between the two LiDAR DSMs (a) and the collapsed building ratio in 57-m grid (b) surveyed by AIJ [26] for the central part of Mashiki Town.

Figure 3 (a) shows the height difference between the pre-main-shock digital surface model (DSM) acquired on April 15, 2016 and the post-main-shock DSM acquired on April 23, 2016. Note that the crustal movements in the main shock were estimated by comparing these two DSMs [20] and they were removed when taking their difference [21]. Figure 3 (b) shows the ratio of collapsed buildings (D5 and D6 in Okada and Takai's damage classification [25]) in a 57 m $\times$ 57 m grid-cell. The damage grades of 2,340 buildings were evaluated by the field surveys of Architectural Institute of Japan (AIJ) [26]. Only the grid cells including equal to or more than 4 buildings were used in calculating the collapsed ratio. The areas along the prefectural road No. 28 were severely damaged with more than 40% collapse ratio.

In order to observe the Pi-SAR2 image in more detail, four typical areas (depicted in Fig. 2 (b)) with the size of 4 grid cells are shown in Fig. 4. The area (a) in the figure is located to the north of the town-hall with four large RC apartment buildings. No apparent building damage can be seen from the aerial photo and the DSM difference although blue chemical sheeting covering damaged roofs are observed for small wooden houses. From the Pi-SAR2 image, the layover of the wall and the radar shadow [27] behind the buildings are clearly seen. It is particularly interesting that each story's wall of the apartment buildings can be recognized.

The area (b) is a built-up residential district with mostly wooden houses. The collapsed ratio (R_c) is low (less than 20 %) and no collapsed building can be seen in the aerial photo. But the shapes of buildings are not so clear in the Pi-SAR2 image for those buildings and thus, it is considered not so easy to detect damage status of wooden houses in Japan, even from very high-resolution airborne post-event SAR images.

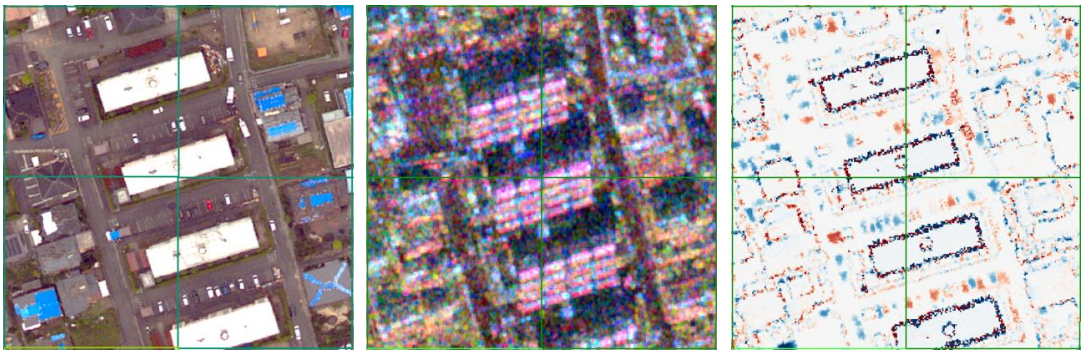

(a) Low collapsed ratio area with RC buildings

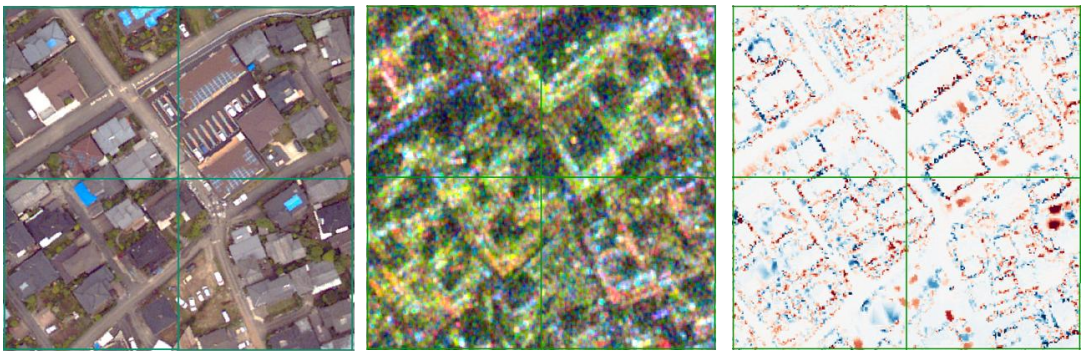

(b) Low collapsed ratio area with wooden houses

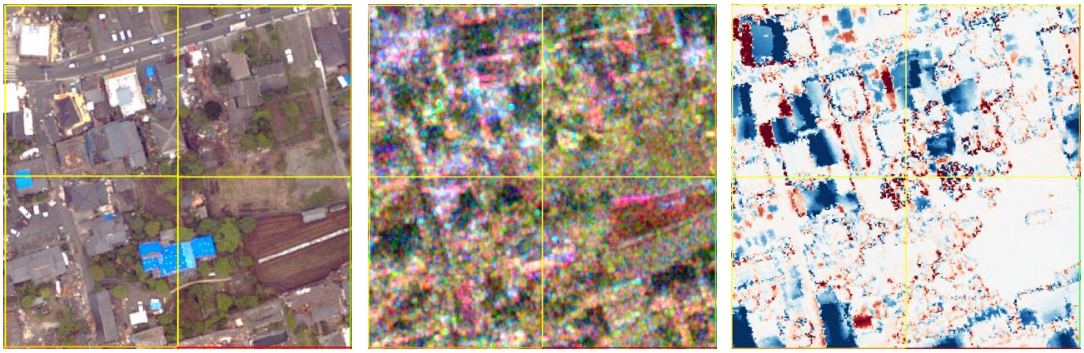

(c) high collapsed ratio area ($R_c \geq 40$ %)

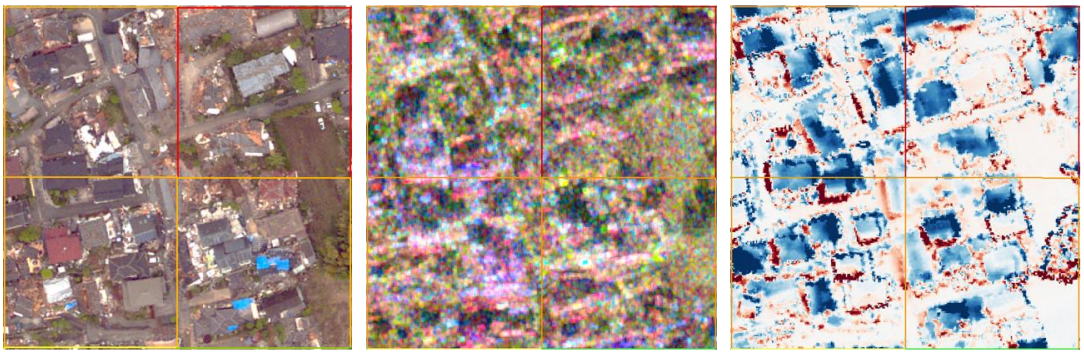

(d) high collapsed ratio area ($R_c \geq 60$ %)

Figure 4. Comparison of enlarged aerial photo (left), Pi-SAR2 color composite (center), and LiDAR DSMs height difference (right) for four typical areas shown in Fig. 2 (b).

The area (c) consists of grid cells with the collapsed ratio larger than 40 %, and the area (d) with the collapsed ratio larger than 60 %. These areas are most severely affected by the Kumamoto earthquake in the town. Mid-story collapse of buildings is most clearly observed by the DSM difference; blue color shows a settlement of about 3 m, corresponding to the collapse of one-story of a wooden house completely. The shapes of collapsed houses are unclear in both the radar shadows and layover areas, which characterizes collapsed buildings and their debris.

But extraction of collapsed buildings only from a one-time SAR image is not an easy task since the radar shadow and layover for a small wooden house are not very distinguishable. The texture of trees around houses makes the task more difficult. Use of texture measures [11] and building footprint data may be considered in the future study for the extraction of collapsed buildings from airborne SAR images of one time-instant.

Conclusions

In this study, airborne SAR images acquired by the National Institute of Information and Communications Technology (NICT), Japan, after the 2016 Kumamoto earthquake were employed to extract collapsed buildings. Soon after the occurrence of the main-shock, Pi-SAR2, an airborne X-band SAR sensor, observed affected areas by the full-polarimetric (HH, HV, VV and VH) mode. A 4-component covariance matrix decomposition was applied to investigate the SAR backscattering characteristics of the affected urban area. The result of the analysis was compared with a damage distribution map obtained by field surveys and airborne LiDAR data. Based on the comparison, radar shadows and layover areas of the Pi-SAR2 data for collapsed wooden houses were seen to be unclear and with irregular shapes, compared with solid undamaged buildings. But more information may be necessary until the extraction of collapsed buildings only from a single SAR image is performed.

Acknowledgments

The Pi-SAR2 images used in this study were owned by National Institute of Information and Communications Technology (NICT), Japan, and were made available through the collaborative research between NICT and Chiba University. This work was partially supported by JST CREST Grant Number JPMJCR1411, Japan, and JSPS KAKENHI Grant Numbers 15K16305 and 17H02066, Japan.

References

1. Yamazaki F, Matsuoka M. Remote sensing technologies in post-disaster damage assessment. *Journal of Earthquakes and Tsunamis* 2007; **1**(3): 193-210.
2. Rathje E, Adams BJ. The role of remote sensing in earthquake science and engineering, opportunities and challenges. *Earthquake Spectra* 2008; **24**(2), 471–492.
3. Eguchi RT, Huyck C, Ghosh S, Adams BJ. The application of remote sensing technologies for disaster management. *The 14th World Conference on Earthquake Engineering* 2008: 17p.
4. Brunner D, Lemoine G, Bruzzone L. Earthquake damage assessment of buildings using VHR optical and SAR imagery. *IEEE Transactions on Geoscience and Remote Sensing* 2010; **48**(5), 2403-2420.
5. Dell'Acqua F, Gamba P. Remote sensing and earthquake damage assessment: Experiences, limits, and perspectives. *Proceedings of the IEEE* 2012: **100** (10), 2876-2890.
6. Liu W, Yamazaki F, Gokon H, Koshimura S. Extraction of tsunami-flooded areas and damaged buildings in the

2011 Tohoku-Oki Earthquake from TerraSAR-X intensity images. *Earthquake Spectra* 2013; **29**(S1), S183-S200.

7. Nakmuenwai P, Yamazaki F, Liu W. Automated extraction of inundated areas from multi-temporal dual-polarization RADARSAT-2 images of the 2011 central Thailand flood. *Remote Sensing* 2017; **9**(1), 78.
8. Yamazaki F, Bahri R, Liu W, Sasagawa T. Damage extraction of buildings in the 2015 Gorkha, Nepal earthquake from high-resolution SAR data. *Proc. of SPIE* 2016, **9877**, 98772K-1-11.
9. JAXA, Pi-SAR, http://www.eorc.jaxa.jp/ALOS/Pi-SAR/about_pisar.html (accessed on 2017/11/5)
10. JAXA, Pi-SAR-L2, http://www.eorc.jaxa.jp/ALOS/Pi-SAR-L2/index.html (accessed on 2017/11/5)
11. Yamazaki F, Samuta N, Liu W. Land-cover classification of suburban areas based on multi-polarized airborne SAR data using texture measures, *Progress in Electromagnetics Research Symposium* 2017; St Petersburg, Russia.
12. Nadai A, Uratsuka S, Umehara T, Matsuoka T, Kobayashi T, Satake M. Development of X-band airborne polarimetric and interferometric SAR with sub-meter spatial resolution. *IEEE International Geoscience and Remote Sensing Symposium* 2009; II-913-916.
13. Susaki J, Kishimoto M. Urban area extraction using airborne X-band fully polarimetric Pi-SAR2 imagery. *International Archives of the Photogrammetry, Remote Sensing and Spatial Information Sciences* 2015; Volume XL-3/W2, 219-226.
14. Geospatial Information Authority of Japan. the 2016 Kumamoto Earthquake. http://www.gsi.go.jp/BOUSAI/H27-kumamoto-earthquake-index.html (accessed on 2017/11/5)
15. Suzuki W, Aoi S, Kunugi T, Kubo H, Morikawa N, Nakamura H, Kimura T, Fujiwara H. Strong motions observed by K-NET and KiK-net during the 2016 Kumamoto earthquake sequence. *Earth, Planets and Space* 2017; **69**(19).
16. Yamazaki F., Liu W., Remote sensing technologies for post-earthquake damage assessment: A case study on the 2016 Kumamoto earthquake. *6th Asia Conference on Earthquake Engineering* 2016; Cebu City, Philippines.
17. Yamazaki F, Kubo K, Tanabe R, Liu W. Damage assessment and 3D modeling by UAV flights after the 2016 Kumamoto, Japan earthquake. *Proceedings of the IEEE International Geoscience and Remote Sensing Symposium* 2017; Fort Worth, Texas, USA, 3182-3185.
18. Liu W, Yamazaki F. Extraction of collapsed buildings due to the 2016 Kumamoto earthquake based on multi-temporal PALSAR-2 data. *Journal of Disaster Research* 2017; **12**(2), 241-250.
19. Zakeri H, Liu W, Yamazaki F. Land cover classification of Kumamoto, Japan using polarimetric decomposition of PALSAR-2 data. *Proc. 38th Asian Conference on Remote Sensing* 2017; New Delhi, India.
20. Moya L, Yamazaki F, Liu W, Chiba T. Calculation of coseismic displacement from Lidar data in the 2016 Kumamoto, Japan, earthquake. *Natural Hazards and Earth System Sciences* 2017; **17**, 143-156.
21. Yamazaki F, Moya L, Liu W. Use of multi-temporal Lidar data to extract changes due to the 2016 Kumamoto earthquake. *Proc. of SPIE* 2017; **10431**, 104310B-1-8.
22. European Space Agency. PolSARpro 5.0 Downloads. https://earth.esa.int/web/polsarpro/download/version-5.0 (accessed on 2017/11/10)
23. Singh G, Yamaguchi Y, Park S. General four-component scattering power decomposition with unitary transformation of coherency matrix. *IEEE transactions on Geoscience and Remote Sensing* 2013; **51** (5), 3014-3022.
24. Asia Air Survey Co., Ltd. the 2016 Kumamoto Earthquake. An approach of crustal deformation analysis based on comparison of two periods of Lidar measurement. http://www.ajiko.co.jp/article/detail/ID5725UVGCD/ (accessed on 2017/11/10)
25. Okada S, Takai N. Damage index functions of wooden buildings and reinforced buildings for seismic risk management. *13th World Conference on Earthquake Engineering* 2004; Paper No. 727.
26. National Institute for Land and Infrastructure Management (NILIM). Quick report of the field survey on the building damage by the 2016 Kumamoto earthquake. Technical Note No. 929 (in Japanese)

http://www.nilim.go.jp/lab/bcg/siryou/tnn/tnn0929.htm (accessed on 2017/11/10)

27. Liu W, Yamazaki F, Sasagawa T. Monitoring of the recovery process of the Fukushima Daiichi nuclear power plant from VHR SAR images. *Journal of Disaster Research* 2016; **11**(2), 236-245.